Relief Gratings on Er/Yb-Doped Borosilicate Glasses and Waveguides by Excimer Laser Ablation

S. Pissadakis[1], *L. Reekie, M. Hempstead*[*], *M.N.Zervas & J.S. Wilkinson*

Optoelectronics Research Centre,

University of Southampton, Highfield, Southampton, SO17 1BJ, UK.

Tel. +44 1703 593954

Fax +44 1703 593149

* Now with SP-TD-01-2, Corning Inc., Corning, NY 14831, USA

Abstract

Relief gratings have been fabricated on Er/Yb-doped borosilicate glass substrates by laser ablation using a 193nm excimer laser and a modified Mach-Zehnder interferometer. The grating fabrication process was quantified using diffraction efficiency measurements and related to the incident energy density. Diffraction efficiencies and grating profiles are presented for gratings fabricated using different pulse energy densities and number of pulses, and optimised fabrication conditions are proposed. Finally, relief gratings were applied to ion-exchanged channel waveguides and spectral transmission measurements are presented.

PACS Codes: 79.20D, 42.40E, 85.40U, 42.82E

Keywords: laser ablation, micromachining, gratings, optical waveguides

---

[1] Corresponding author. Optoelectronics Research Centre, University of Southampton, Highfield, Southampton, SO17 1BJ, UK. Tel. +44 1703 593954, Fax +44 1703 593149, E-mail: sp1@orc.soton.ac.uk

1 INTRODUCTION

The use of excimer lasers for fine machining of optical materials has demonstrated increasing potential in recent years. For fine structure patterning, direct UV-VUV ablation machining offers several advantages over other patterning methods such as photo- or e-beam lithography. The excellent etching quality and the single-step nature of the process have established excimer laser ablation as a promising micro-fabrication technique.

The UV ablation behaviour of polymers [1, 2], crystals [3, 4, 5], and amorphous optical materials [6] have been studied extensively with regard to laser wavelength and energy fluence, and machining techniques such as multi-pulse exposure and chemically-assisted ablation have been investigated. For amorphous materials, especially for glass, fine quality imprinting has been reported using wavelengths of 308nm [7], 248nm [8, 9] and 193nm [9, 10, 11]. It has been found that glass ablation using a 193nm excimer laser produces structures of high smoothness without generating extensive surface damage in the form of cracks, in contrast to the effects of ablation at 248nm. Furthermore, the ablation threshold, defined as the minimum energy density required to induce uniform ablation using a specific number of pulses, is significantly lower using radiation at a wavelength of 193nm compared with that at a wavelength of 248nm.

These studies of the interaction between glass and intense UV radiation have prompted the development of excimer laser micro-machining as a reliable and effective fabrication technique for sub-micron structures, and gratings in particular. High quality relief gratings overlaid on

dielectric waveguides may play a significant role in integrated optics, particularly in the context of devices for wavelength-division multiplexed (WDM) optical fibre systems [12]. Since surface relief gratings may exhibit strong interaction with waveguide modes, they can provide efficient wavelength-dependent coupling between backward or forward travelling modes in waveguide structures, allowing wavelength filtering functions to be realised. A particular benefit of relief gratings is their easy application to the majority of optical materials, in contrast with photorefractive gratings, which are applicable to a very limited range of materials. Further advantages include their excellent temperature stability and the absence of any significant ageing problems. Relief gratings fabricated using UV ablation have been reported on polymer [13] and silicon [14] substrates using 248nm injection cavity excimer lasers, and on polymers using a 193nm excimer laser and a Talbot interferometric configuration [10, 15].

In this paper we report the fabrication of relief gratings in borosilicate glass using holographic ablation, with an excimer laser at a wavelength of 193nm, under atmospheric pressure conditions. The typical three-mirror interferometer shown in Figure 1 was used to produce high-intensity UV fringes on the sample surface and consequently cause ablation. The substrate material was an Er/Yb co-doped borosilicate glass, which may be employed in optical telecommunication applications as a host for waveguide amplifiers [16] or lasers [17]. The principal studies concerned Bragg gratings with a period near 500nm for potential application in sources for 1.5μm telecommunications systems. Sub-micron relief structures may also be fabricated on this scale using UV, X-ray or e-beam lithography, but excimer laser ablation has the advantage that it is a single step process, resulting in reduced fabrication complexity. Writing

of gratings on bulk glass samples was used to characterise the ablation process for future work on waveguide gratings. The relationship between the energy density, the number of pulses and the diffraction efficiency of the relief gratings was determined. Holographically-ablated gratings were written on thallium ion-exchanged Er/Yb-doped borosilicate glass waveguides and polarisation-resolved spectral measurements of the resultant waveguide filters are presented. Problems encountered with cracking of the ion-exchanged regions in channel waveguide structures during laser ablation are also discussed.

2 EXPERIMENTAL

2.1 Initial sample preparation

The borosilicate glass samples and waveguides used throughout this study were prepared by Corning Europe. The glass substrates (50 x 50 x 3mm) were optically polished and had a composition of approximately 63wt% SiO_2, 10wt% B_2O_3, 9wt% Na_2O, 7wt% K_2O, 2wt% BaO, 5wt%Yb_2O_3, 3wt% Er_2O_3, and 1wt% trace compounds.

Straight channel waveguides were formed in one substrate by thallium (Tl^+) ion exchange after photolithographic definition of a diffusion mask. A series of channel waveguides was initially realised in the samples by ion exchange in a pure thallium salt bath through openings in the mask ranging from 2.5μm to 4μm in width. This primary ion exchange was performed at 400°C for a duration of 1.5 hours. The channels were buried below the sample surface, to minimise losses

and improve waveguide symmetry, during a second field-assisted ion-exchange step [16]. The resultant mode dimensions at the $1/e^2$ normalised intensity point for a waveguide channel fabricated by diffusion through a 3μm opening in the mask are 6.3μm parallel to the surface and 4μm in depth, at a wavelength of 1310nm [18]. After ion exchange the waveguide ends were optically polished, to allow end-fire coupling of light from a lens or optical fibre, resulting in a final length of 40mm.

2.2 Interferometer configuration

A line-narrowed injection cavity excimer laser operating at a wavelength of 193nm (Lambda Physik EMG 150) was set up to produce coherent pulses of approximately 120mJ energy and FWHM duration 22ns. The dimensions of the output beam were 0.7cm x 1.3cm. The apparatus used to expose the substrates to the radiation is shown in Figure 1. The laser output (1) was focused onto the glass sample using a two-lens cylindrical telescope (2) allowing the beam area on the sample to be adjusted. The beam was then divided by a beam splitter (3) and reflected from three mirrors (4) onto the sample being exposed (5). A fused silica plate (6) was placed in the two-mirror interferometer branch to achieve optical path compensation. The three-mirror approach was used to avoid wavefront inversion at the sample, which is necessary since the excimer laser beam has a low spatial coherence. Although the beamsplitter provided a power splitting ratio of 50:50 at a wavelength of 193nm, the resultant energy density ratio on the sample surface was found to be approximately 35:65, due to the larger number of reflections in the path of one of the interfering beams. The maximum energy density in the bright fringes of

the interference pattern can be evaluated using the standard interference fringe contrast equations and the energy density of the two beams. For the present conditions this maximum energy density is almost twice the sum of the individual beams densities. The experimental apparatus was laid out on a vibration-isolated table and placed in a sealed box in order to eliminate any air currents. The total energy per pulse incident upon the sample ranged between 5mJ and 35mJ.

2.3 Grating exposure

The first series of gratings was written using single-pulse exposures with the excimer laser beam focused on the glass sample surface to an area of approximately 250μm by 1.3cm and with a periodicity of 500nm. The excimer laser beam was not homogenized, since this would significantly reduce the spatial coherence of the beam, resulting in non-optimum grating recording. The energy density profile of the beam before the interferometer showed variations less than 10% of the average value measured using a pyroelectric energy meter. A wide variety of gratings were recorded for single-pulse energy densities varying between 0.2J/cm^2 and 1.1J/cm^2 where the exposed area was kept constant. The energy of each pulse was monitored on-line by measuring a backreflection from a mirror into the interferometer. Subsequently, exposures of five, ten and twenty pulses were carried out using a repetition rate of 0.5Hz. In this case the power density was adjusted by altering the exposed area, without changing the laser pulse energy. It has been reported [6, 11] that each pulse alters the ablation characteristics of the remaining material for subsequent pulses, and the purpose of this part of the study was to investigate the role of these "incubation" phenomena [11] on the grating growth process. The

laser repetition rate was kept low to avoid plume screening of the laser beam and also to minimise thermal effects. Finally, five-, ten- and twenty-pulse gratings were patterned on the waveguide sample with average single-pulse energy densities between 0.57J/cm^2 and 0.68J/cm^2. The waveguide gratings fabricated here are intended to operate as strongly wavelength-selective reflective Bragg gratings close to wavelengths for optical fibre communication systems. In order to avoid the Er^{3+} absorption band in the glass at wavelengths close to 1.5μm, grating recording was shifted to the 1300nm band by selecting a grating period of approximately 426nm. The grating period was confirmed by recording a reflection grating in a photosensitive fibre of a characterized effective refractive index and checking the spectrum of the back reflection using an optical spectrum analyser.

2.4 Grating characterisation

2.4.1 Undiffused samples

The gratings etched on the undiffused substrates were characterized using a diffraction efficiency measurement with the configuration of Figure 2. A linearly polarised He-Ne beam (1) was focused on the grating surface using a x10 objective lens (2). The diffraction efficiency measurements were taken in the center of the exposed area. The focused He-Ne beam was scanned along the width of the ablated grating and refocused to cover the whole grating width until no diffraction fringes (produced by the grating area borders) were visible. The final measurement position determined where the signal of the +1-diffracted order was maximised.

The sample plane (3) was tilted with respect to the He-Ne beam until the first diffraction order appeared in transmission (4). The first diffracted order was collected using another objective (5) and directed to a power meter (6) through an aperture to reduce stray light. In the ideal case the grating depth, d, may be found from the diffraction efficiency η by Equation 1 [19]:

$$d = \arcsin(\sqrt{\eta})\ \frac{\lambda \cos\theta_0}{\pi \Delta n} \cong \sqrt{\eta}\ \frac{\lambda \cos\theta_0}{\pi \Delta n} \qquad 1$$

where λ is the free-space wavelength, $\cos\theta_0$ is the Bragg angle, and Δn is the refractive index difference between the surrounding medium and the grating. Equation (1) has been derived assuming an incident plane wave and is valid for thin gratings where η is small and no absorption is present. In the present case a diverging beam is diffracted from the grating structure and the power of the diffracted orders is measured with respect to the incident power, corrected for Fresnel reflections, and then used for diffraction efficiency determination. Components of the incident radiation incident at angles other than the Bragg angle will be diffracted with lower efficiency, resulting in an underestimate of the grating depth. Furthermore it is expected that, at UV-writing energies below the ablation threshold and in regions remaining after ablation, the physical properties of the glass will be altered, resulting in a photorefractive or loss grating. This will result in measurable power in the diffraction order even when no relief grating has been formed. However, the simple measurement procedure described may be used to gain an estimate of relative grating strength. In order to obtain precise measurements of local grating depth, atomic force microscopy (AFM) was used to measure the local grating height for comparison with diffraction measurements, and scanning electron microscopy (SEM) was used to study the general structure of the gratings. An absolute measurement of the grating depth

using only the AFM scans is not feasible. Localised irregularities and microscopic non-uniform ablation -due to the beam profile fluctuations ("hot spots") produce results with large deviations between them. The diffraction efficiency measurements may provide an underestimate of the actual grating depth but have the advantage of averaging over large grating areas.

2.4.2 Waveguide samples

The gratings etched on the substrates in which waveguides had been realised were characterised using the apparatus shown in Figure 3. Light from a 1300nm broadband LED source pigtailed with a single-mode fibre (1) was coupled into a single-mode high-birefringence (Hi-Bi) fibre using a system of two 10x low birefringence objectives lenses (2). A rotatable IR polariser (3) was positioned between the two objective lenses to provide linear polarisation and allow alignment parallel to the fast or slow optical axis of the Hi-Bi fibre (4). The output end of the Hi-Bi fibre was mounted in a precision rotation v-groove and butt-coupled to the waveguide to allow TE or TM polarised excitation (5). Finally, a standard single-mode fibre (6) was end-coupled to the waveguide output to collect the output radiation and guide it to an optical spectrum analyser (7), which recorded the spectrum of the light emerging from the waveguide. Input coupling was optimised by maximising the power emerging from the waveguide, resulting in the preferential excitation of the fundamental mode at wavelengths where these waveguides are dual-moded. A subsequent measurement was made with the waveguide removed to allow the spectral transmission of the waveguide alone to be deduced. The transmission measurement was separately normalised for each polarisation to the power emerging from the input fibre, and

therefore includes input coupling and propagation losses in addition to the grating reflection characteristics. The use of a 1300nm Hi-Bi fibre at the waveguide input allowed polarisation-resolved measurements to be made, while use of a standard single-mode fibre at the waveguide output reduced interference from light unintentionally launched into the substrate.

3 RESULTS

3.1 Single-exposure gratings

The measured diffraction efficiency and the average grating depth calculated using Equation 1 are plotted against energy density in Figures 4 and 5, respectively. Inspection of the samples showed that uniform grating ablation, characterised by smooth even lines, starts at an energy density of 0.6J/cm^2 for single pulse exposure; below this threshold the exposed areas appeared to be damaged rather than removed. The ablation threshold for the grating fabrication was determined from the diffraction efficiency measurements and confirmed by optical microscope examination and AFM scanning of the treated area. Following this classification process, high damage volume gratings comparable to Type II gratings observed in optical fibres [20] could be distinguished from shallow relief gratings on the exposed material. The maximum grating depth (averaged value) for single-pulse exposure, estimated from diffraction measurements, was approximately 35nm and was obtained with an energy density of 1.1J/cm^2. An AFM image taken from the centre of the exposed grating area of this sample is shown in Figure 6. A cross-

section of the grating grooves obtained by AFM is shown in Figure 7. The maximum grating depth measured in this region of 10mm x 0.25mm was 130nm. As this value was measured in the centre of the exposed grating area, where the interfering beams have their maximum, it represents the maximum grating depth on the sample. The grating period was found to be 494±8nm, in good agreement with the initial design value of 500nm.

3.2 Multiple-exposure gratings

Diffraction efficiency measurements were carried out for the samples exposed to multiple pulses and the calculated grating depth against average energy density per pulse is presented in Figure 8. By comparing Figures 5 and 8 it can be seen that the grating ablation threshold per pulse reduces for a greater number of pulses. For single pulse exposure, 0.6J/cm^2 was needed to initiate ablation, 0.55J/cm^2 for 5 pulses, 0.4J/cm^2 for 10 pulses and 0.36J/cm^2 for 20 pulses. These ablation thresholds were extracted using the diffraction efficiency data and are not expected to be valid for non-interferometric ablation where no structural pattern is created.

For 5-pulse exposures the grating growth increases with the energy density. In the case of gratings formed by 10- and 20-pulse exposures, a maximum in the curves of diffraction efficiency against energy density appears for energy densities not far above the ablation threshold. The reduction in grating strength for higher energy densities may result from accumulated material damage due to the increased exposure. For multi-pulse (five, ten and

twenty pulse) exposed gratings higher diffraction orders are also observed. It is believed that this may be attributed to the formation of gratings with groove profiles containing strong Fourier orders at spatial frequencies higher than the fundamental.

Figure 9 shows a scanning electron micrograph of a grating fabricated using 5-pulse exposure and an average pulse energy density of 0.55 J/cm^2. The machining appears uniform and of high quality and the density of particulate matter attached to the surface is low. A higher energy density would yield a deeper grating, however it was found that exposure to a higher energy density resulted in a poor surface with a higher density of particles of ablated glass deposited on the machined area.

3.3 Gratings exposed on waveguides

The grating period on the waveguide sample measured by atomic force microscopy was found to be 417±8nm (AFM measurement), marginally shorter than the target value of 426nm. Transmission spectra for both TE and TM polarisation, for a waveguide in which a grating was written using 10 pulses of average energy density 0.612J/cm^2 are shown in Figure 10. Polarised transmission spectra for a similar waveguide on the same substrate on which a grating has not been written are also given. The waveguides under study were ion-exchanged through a channel opening in the mask of nominal width 4μm, the grating length was 6mm and the average depth, as predicted from Figure 8, was approximately 50nm. The curves are corrected for the spectral response of the measurement system but include fibre-waveguide coupling losses and waveguide

propagation losses. In the case of the waveguide without an ablated grating it can be seen that the total loss is of order 4-5dB over the spectral window of interest; it is believed that this is dominated by fibre-waveguide coupling losses, which have not been optimised. At a wavelength of 1300nm these waveguides, designed for operation at 1500nm, support two modes in both polarisations.

In the case of the TM polarisation, the transmission spectra of the grating waveguides exhibit two notches due to the dual-moded nature of the waveguide at the reflection wavelengths. These notches are located at 1274nm (Notch I) and 1264nm (Notch II) and are attributed to coupling from the forward fundamental mode to the backward travelling fundamental and first-order guided modes, respectively. The maximum grating extinction ratio, which occurs for Notch II, is approximately 28dB with respect to transmission away from the grating band, although this measurement is limited by instrumental resolution. This notch has a bandwidth of 6nm at FWHM, which appears to be broader than similar Type II damage gratings [20]; such broadening can be attributed to non-uniform ablation along the length of the grating. Notch I, due to the fundamental mode, has a depth of 19dB. Adjusting the input fibre position relative to the waveguide input alters the excitation of the individual modes, resulting in variations of the relative strength of the observed notches. For the TE polarisation the effect of the grating is significantly decreased, due to the reduced overlap between the guided fields and the grating region in this birefringent waveguide [21]. The two grating peaks that correspond to the first order and fundamental guided modes are now located at 1266nm and 1273nm respectively.

The transmission spectra for the waveguides containing an ablated grating exhibit additional broadband losses of approximately 11dB, and ripple of a few dB, over the spectral window of interest, when compared with the non-irradiated waveguides. The broadband loss corresponds to approximately 2dB/mm of grating length and is due to micro-cracks observed between the ion-exchanged and undoped sample area. It is believed that these cracks occur during ablation on ion-exchanged waveguides due to the stress introduced by the in-diffused ions. The origin of the spectral ripple is presently unknown.

4 DISCUSSION

4.1 Grating ablation in undiffused bulk samples

The physical background of glass ablation has been studied in depth elsewhere [6, 8, 9]. UV ablation of glass is dominated by strong glass absorption at wavelengths below 320nm, corresponding to a photon energy of approximately 3.9eV. The photon energy of the 193nm radiation is about 6.4eV, resulting in strong surface absorption and ablation at low pulse energy density. A simple theory for the ablation process, using an absorption model, can be represented by the Equation 2 [9]:

$$d_{etch}(F) = 1/\alpha \ln(F/F_t) \qquad 2$$

where d_{etch} is the etch depth, α is the absorption at the specific wavelength, F is the pulse energy

fluence and F_t is the energy fluence at the ablation threshold. In the case of interference the factor F is not a solid number but is described by the interference pattern equation, resulting to an intensity modulation.

Estimation of diffraction efficiency for single-pulse exposures given in Figure 4 shows that grating strength grows with pulse energy, as expected, and that there is a threshold energy density before a grating can form. However, inspection of the gratings shows that, at energy densities below $0.5J/cm^2$, grating formation is due to photorefractive or damage effects rather than writing of a relief grating. The single-pulse threshold for volume damage gratings is approximately $0.2J/cm^2$ and that for ablated gratings is approximately $0.55J/cm^2$.

Similar measurements for gratings formed by multiple-pulse exposures show that for 10 pulses a maximum grating strength is achieved at an average single-pulse energy density close to the ablation threshold. It is believed that the grating strength does not continue to grow with higher energy densities due to incubation effects and diffused thermal phenomena, where exposure during earlier pulses damages the glass and alters the ablation threshold for subsequent pulses. The contrast of the interferometric fringes is approximately 0.95, which minimizes the possibility of ablation from the "dark" lines as well as from the "bright" lines of the pattern, leading to a reduced grating contrast, in case where multi-pulse exposures are used. Changes of the interference pattern due to surface modification while material is removed may result in alterations of the energy density over the grating length, affecting the grating contrast. In the case of the 20-pulse exposures the incubation effects are more pronounced and, combined with

energy density redistribution phenomena -due to surface modification as mentioned above-, reduced grating strength is achieved. These results lead to the choice of 10 pulses of 0.6J/cm^2 as the optimum grating writing conditions for this glass using our apparatus.

4.2 Gratings ablated on waveguide samples

Gratings of an average predicted depth of 50nm and a length of 6mm were ablated directly on thallium ion-exchanged waveguides in Er/Yb-doped borosilicate glass. The waveguide transmission spectra exhibited stop-bands at around 1.3μm having extinction greater than 25dB in the TM polarisation and greater than 5dB in the TE polarisation. These results indicate that strong gratings may readily be written in glass waveguides using this technique. The difference between the grating strength for the two polarisations is primarily due to reduced modal field strength at the surface for the TE polarisation. The waveguides were designed to operate in the 3rd telecommunications window at around 1550nm; however, to avoid the erbium absorption, the gratings were written for wavelengths around 1300nm where the waveguides are dual-moded, resulting in dual stop-bands in the transmission spectrum. Observation of two strong stop-bands is possible due to the preferential excitation of the fundamental mode by the input fibre. The stop-band wavelengths for the two polarisations do not coincide, due to waveguide anisotropy including geometrical and stress effects. Polarisation insensitivity is not required for the realisation of DFB waveguide lasers in Er/Yb glass where gratings may be designed for the polarisation of interest.

In addition to the narrowband reflection notches caused by the grating, a broadband loss of 2dB per mm of grating has been introduced, compared with the waveguides that have not been exposed to UV. Inspection of the waveguides revealed evidence of significant microcracking along the thallium ion-exchanged waveguide regions, which causes scattering losses and which may be due to stress introduced by diffusion of the thallium ions. Work is in progress to write gratings in films with a lower ablation threshold deposited on these waveguides, to avoid microcracking.

In the present work, the combination of a short-wavelength laser and an interferometric apparatus allows precise micro-machining of borosilicate glass, which has a high ablation threshold relative to other optical materials. The use of a wavelength of 193nm has the advantage of high quality etching of the glass, which is not easily realised using 248nm radiation. Furthermore the reduced ablation threshold of the glass at 193nm compared to 248nm allows easier imprinting of larger area gratings, having the same laser output for the two wavelengths. A significant advantage of interferometric ablation over other excimer laser ablation techniques is the ready tunability of the recorded grating period by straightforward adjustment of the interferometer.

5 SUMMARY

Direct etching of relief gratings in Er/Yb-doped borosilicate glass using 193nm excimer laser

holography is reported. The grating ablation process was studied as a function of energy fluence and number of pulses and gratings of maximum depth 140nm having a period of 500nm or less are reported. The ablation processes involved in grating writing are examined and related to the experimental data. The sensitivity of the grating ablation process to the machining conditions is described and optimum fabrication conditions for surface gratings are proposed. Additionally, the role of the multi-pulse effects are examined and correlated with the grating growth. Gratings were written on Tl^+ ion-exchanged waveguide channels in Er/Yb borosilicate glass in order to demonstrate spectral filtering. Despite problems with waveguide cracking, a waveguide grating operating near 1300nm, having an extinction of >28dB and a bandwidth of 6nm for the TM polarisation was realised.

6 ACKNOWLEDGEMENTS

The authors acknowledge the EU ACTS project TOBASCO (Towards Broadband Access Systems for CATV Optical Networks) for financial support and Corning Europe for supplying the Er/Yb-doped glass and waveguides and supporting information. Thanks are also due to Ms P.Hua for the SEM pictures and Dr W.S. Brocklesby for the AFM scans. The Optoelectronics Research Centre is an Interdisciplinary Research Centre funded by the UK Engineering and Physical Sciences Research Council.

7. REFERENCES

1. T.J. Chuang, H. Hiraoka, and A. Modl, Laser-photoetching characteristics of polymers with dopants, Appl. Phys. A45, 277-288, 1988

2. N.A. Vainos, S. Mailis, S. Pissadakis, L.Boutsikaris, P.J.M. Parmiter, P. Dainty, and T.J. Hall, Excimer laser use for microetching computer-generated holographic structures, Appl. Opt., vol. 35, 32, 6304-6319, 1996

3. A.C. Tam, J.L. Brand, D.C. Cheng, and W. Zapka, Picosecond laser sputtering of sapphire at 266nm, Appl. Phys. Lett. 55, 2045-2047, 1989

4. S. Preuss and M. Stuke, Subpicosecond ultraviolet laser ablation of diamond: Nonlinear properties at 248nm and time-resolved characterization of ablation dynamics, Appl. Phys. Lett. 67, 338-340, 1995

5. M. Eyett and D. Bauerle, Influence of the beam size on ablation rates in pulsed-laser processing, Appl. Phys. Lett. 51 (24), 2054-2055, 1987

6. B. Braren and R. Srinivasan, Controlled etching of silicate glasses by pulsed ultraviolet laser radiation, J. Vac. Sci. Technol. B6 (2), 537-541, 1988

7. C. Buerhop, B. Blumenthal, R. Weissmann, N. Luntz ans S. Biermann, Glass surface treatment with excimer and CO_2 lasers, Appl. Surf. Sci. 46, 430-434, 1990

8. J. Ihlemann, B. Wolff-Rottke, Excimer laser micro machining of inorganic dielectrics, Appl. Surf. Sci. 106, 282-286, (1996)

9. S.R. Jackson, W.J. Metheringham, P.E. Dyer, Excimer laser ablation of Nd:YAG and Nd:glass, Appl. Surf. Sci. 86, 223-227, 1995

10. P.E. Dyer, R.J. Farley, R. Giedl, D.M. Karnakis, Excimer laser ablation of polymers and glasses for grating fabrication, Appl. Surf. Sc., 96-98, 537-549, 1996

11. J. Ihlemann, B. Wolff, and P. Simon, Nanosecond and femtosecond excimer laser ablation of fused silica, Appl. Phys. Lett. A 54, 363-368, 1992

12. C. P. Hussell and R.V. Ramanswamy, High-index overlay for high reflectance DBR gratings in LiNbO3 channels waveguides, IEEE Phot. Tech. Lett. V.9, 636-638, 1997

13. K. J. Ilcisin and R. Fedosejevs, Direct production of gratings on plastic substrates using 248-nm KrF laser radiation, Appl. Opt. 26, 396-400, 1987

14. R. Fedosejevs, M.J. Brett, Direct formation of grating structures on silicon using KrF laser radiation, Appl. Opt. 28, 1877-1880, 1989

15. P.E. Dyer, R.J. Farley, R. Griedl, Analysis and application of a 0/1 order Talbot interferometer for 193nm laser grating formation, Opt. Comm. Q129, 98-108, 1996

16. P. Camy, J.E. Roman, F.W. Willems, M. Hempstead, J.C. van der Plaats, C. Prel, A. Beguin, A.M.J. Koonen, J.S. Wilkinson and C. Lerminiaux, Ion-exchanged planar lossless splitter at 1.5μm, Electr. Lett. V.32, 321-322, 1996

17. J.E. Roman, P. Camy, M. Hempstead, WS Brocklesby, S. Noah, A. Beguin, C. Lerminiaux and J.S. Wilkinson, Ion-exchanged Er/Yb waveguide laser at 1.5μm pumped by laser diode, Electr. Lett. v.31, 1345-1346, 1995

18. Progress reports, European Union RACE Project R2109: LIASON, Deliverables 7, 11

19. H.M. Smith, Holographic Recording Materials, v.20, Eds. H.M. Smith (Springer-Verlag, New York, 1977)

20. J.L. Archambault, L. Reekie, P.St.J. Russell, 100% reflectivity Bragg reflectors produced in

optical fibres by single excimer laser pulses, Electron. Lett. 29, 453-454, 1993

21. K.A. Landa, L.M. Landa, A.V. Mishin, G.T. Petrovskii, Anisotropic Tl^+ diffusion waveguides in optical-glass, Doklady Akademii NAUK SSSR, 269, 1355-1357, 1983

8 FIGURE CAPTIONS

1. Excimer laser ablation interferometer.

2. Experimental apparatus for the measurement of the diffraction efficiency of ablated gratings.

3. Apparatus for the polarisation-resolved measurement of waveguide transmission spectra.

4. Diffraction efficiency vs pulse energy density for ablated gratings. Point A: Single-pulse ablation threshold.

5. Average grating depth vs energy density, evaluated using diffraction efficiency measurements. Point A: Single-pulse ablation threshold.

6. Atomic force micrograph (AFM) image of a grating ablated using a 193nm excimer laser.

7. AFM cross-section of the ablated grating shown in Fig 6.

8. Average grating depth vs average single-pulse energy density, for ablated gratings fabricated using multi-pulse exposures. a: 5 pulses, b: 10 pulses, c: 20 pulses. The lines are solely an aid to observe the trends, and do not represent a numerical fit.

9. SEM image of excimer laser ablated grating fabricated using a five-pulse exposure and an average energy density of $0.55J/cm^2$.

10. Waveguide transmission spectrum of a Tl^+ ion-exchanged waveguide incorporating an ablated grating with an air superstrate. UW: unexposed waveguide spectra, GW: grating waveguide spectra. Solid lines: TM polarization. Dashed lines: TE polarization.

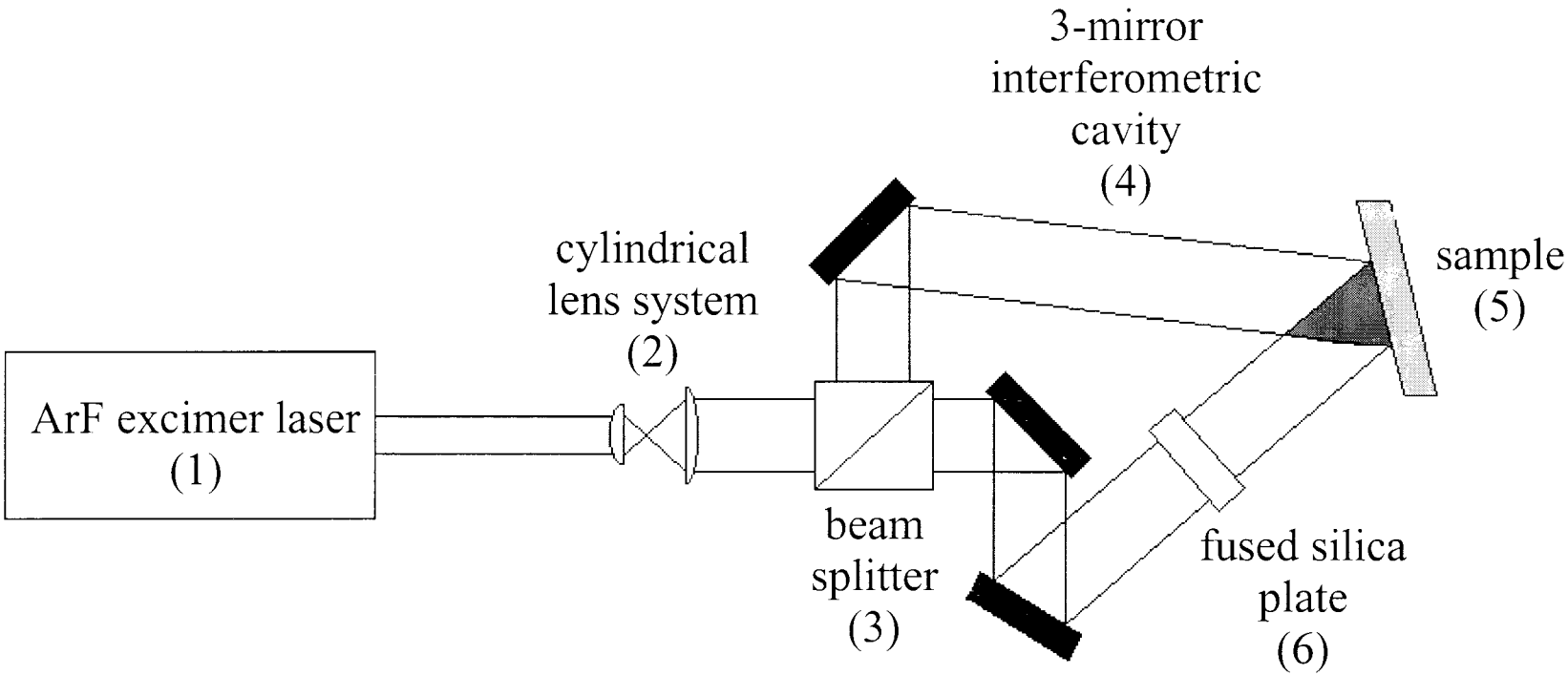
3-mirror
interferometric
cavity
(4)
cylindrical
lens system
(2)
sample
(5)
ArF excimer laser
(1)
beam
splitter
(3)
fused silica
plate
(6)

Fig. 1

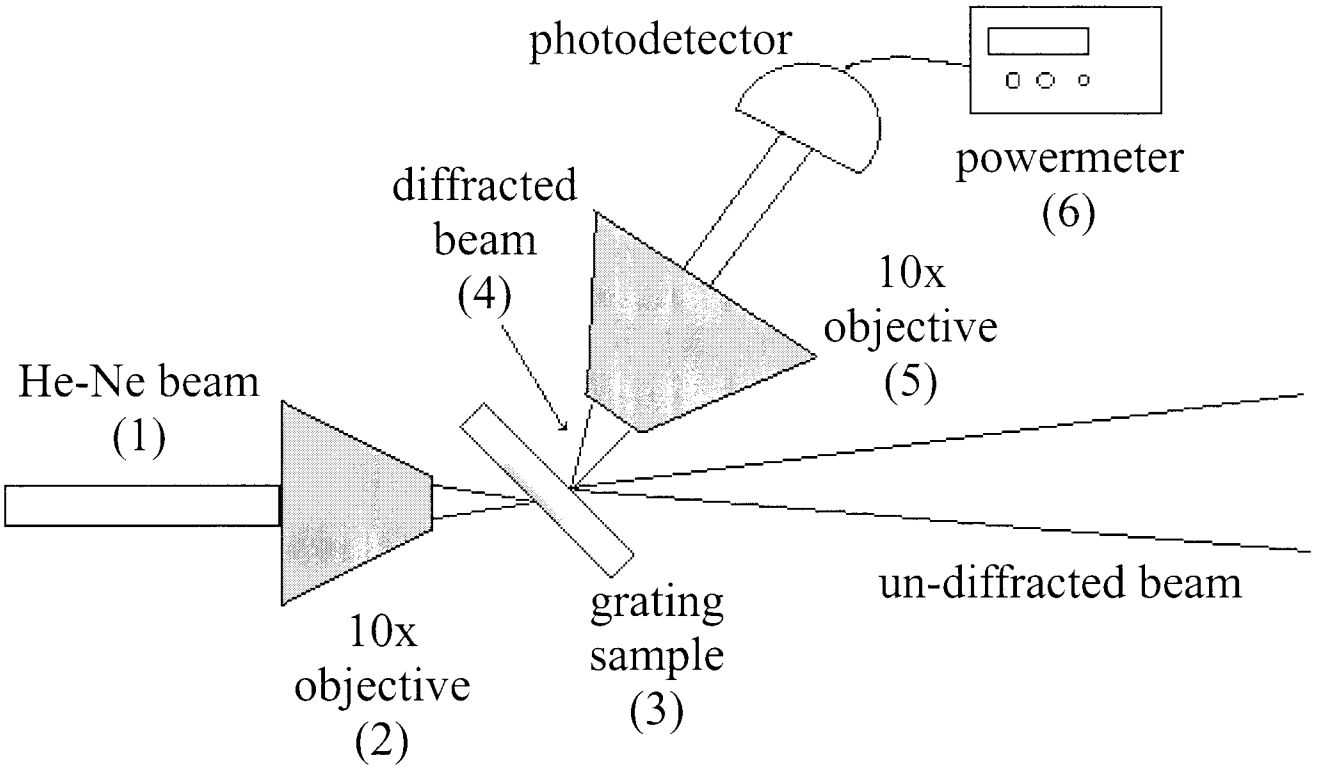
photodetector
powermeter
(6)
diffracted
beam
(4)
10x
objective
(5)
He-Ne beam
(1)
10x
objective
(2)
grating
sample
(3)
un-diffracted beam

Fig 2

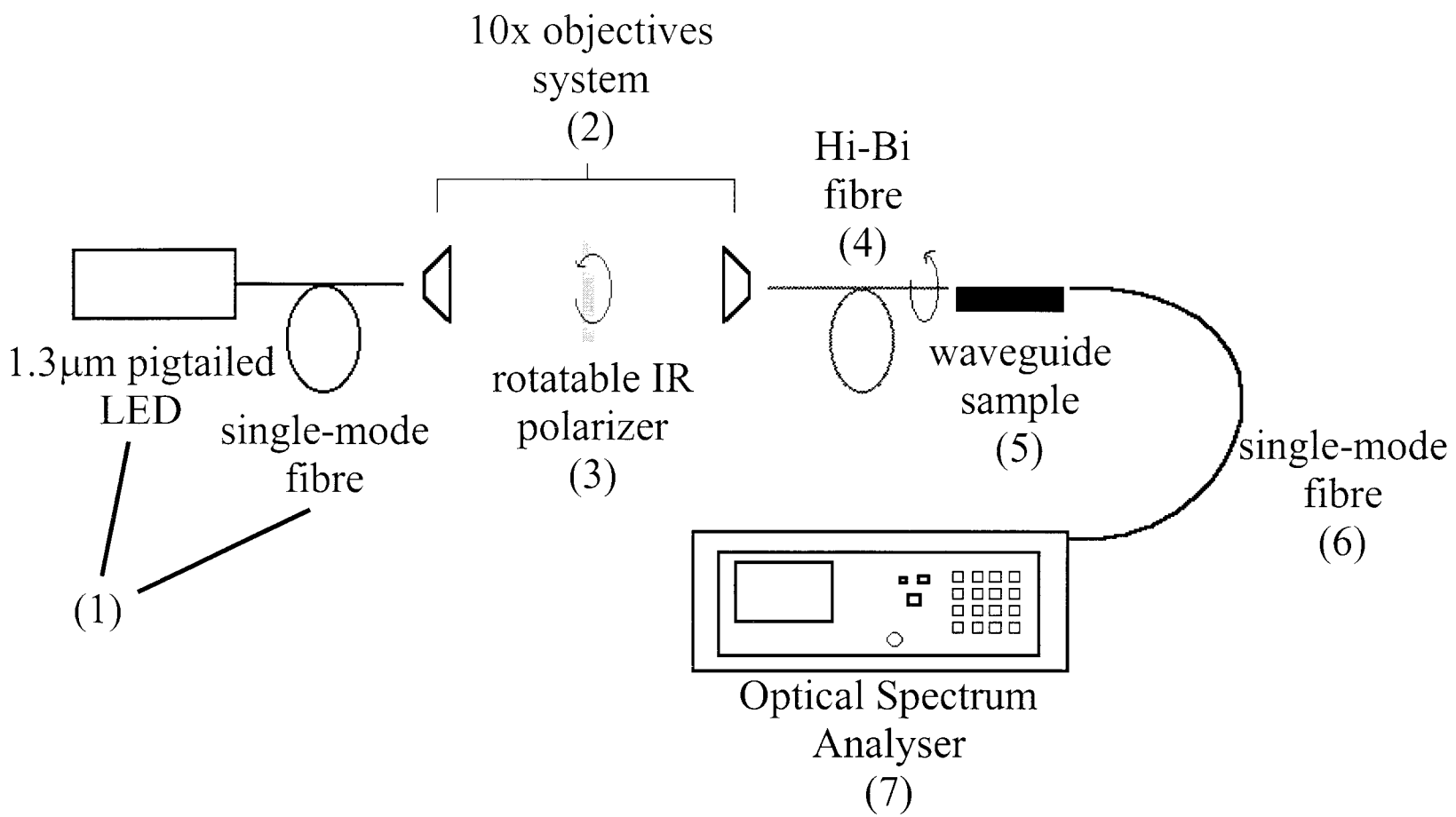
10x objectives
system
(2)
Hi-Bi
fibre
(4)
1.3μm pigtailed
LED
single-mode
fibre
rotatable IR
polarizer
(3)
waveguide
sample
(5)
single-mode
fibre
(6)
(1)
Optical Spectrum
Analyser
(7)

Fig. 3

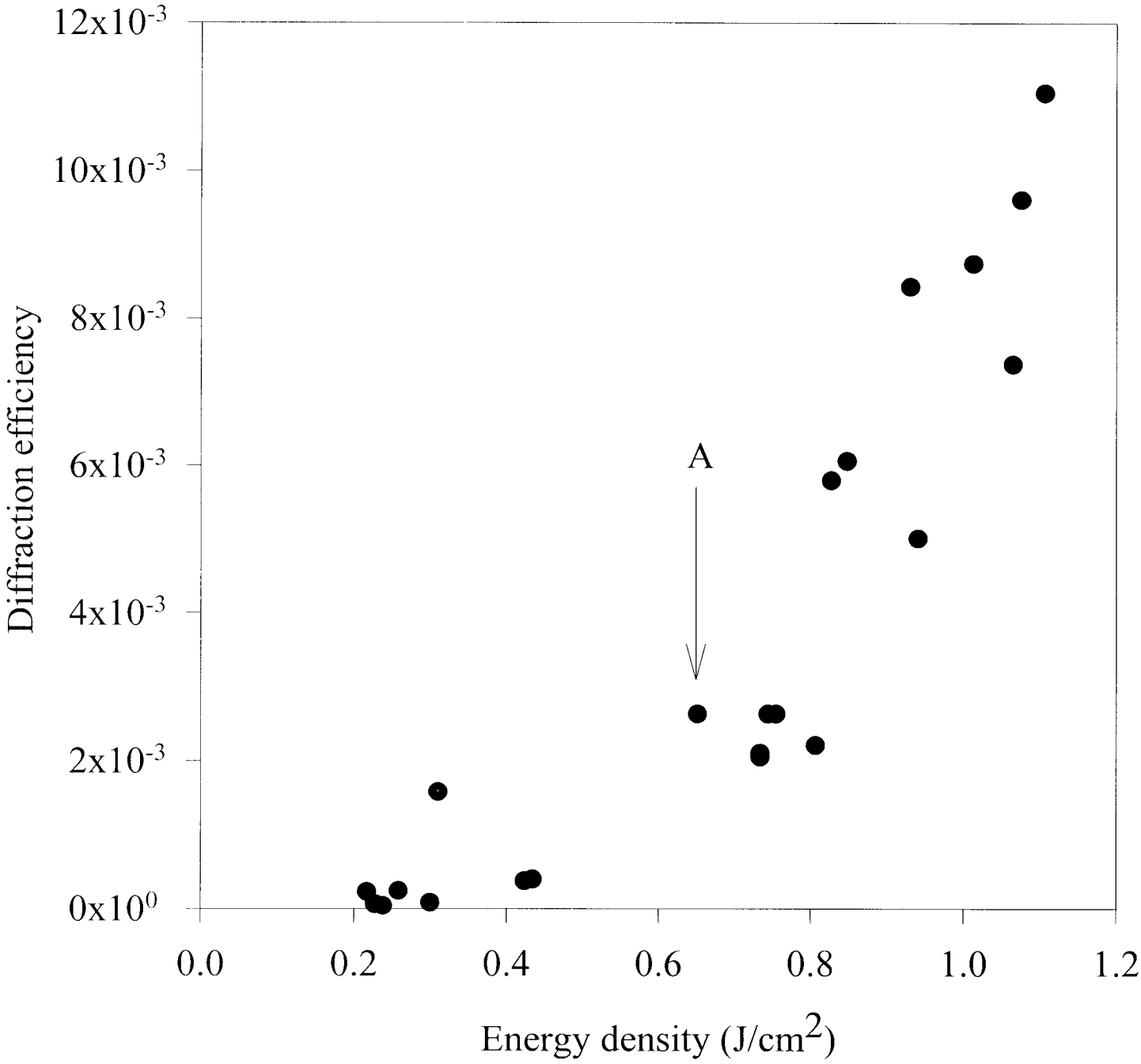
12x10-3
10x10-3
8x10-3
6x10-3
4x10-3
2x10-3
0x100
Diffraction efficiency
A
0.0
0.2
0.4
0.6
0.8
1.0
1.2
Energy density (J/cm2)

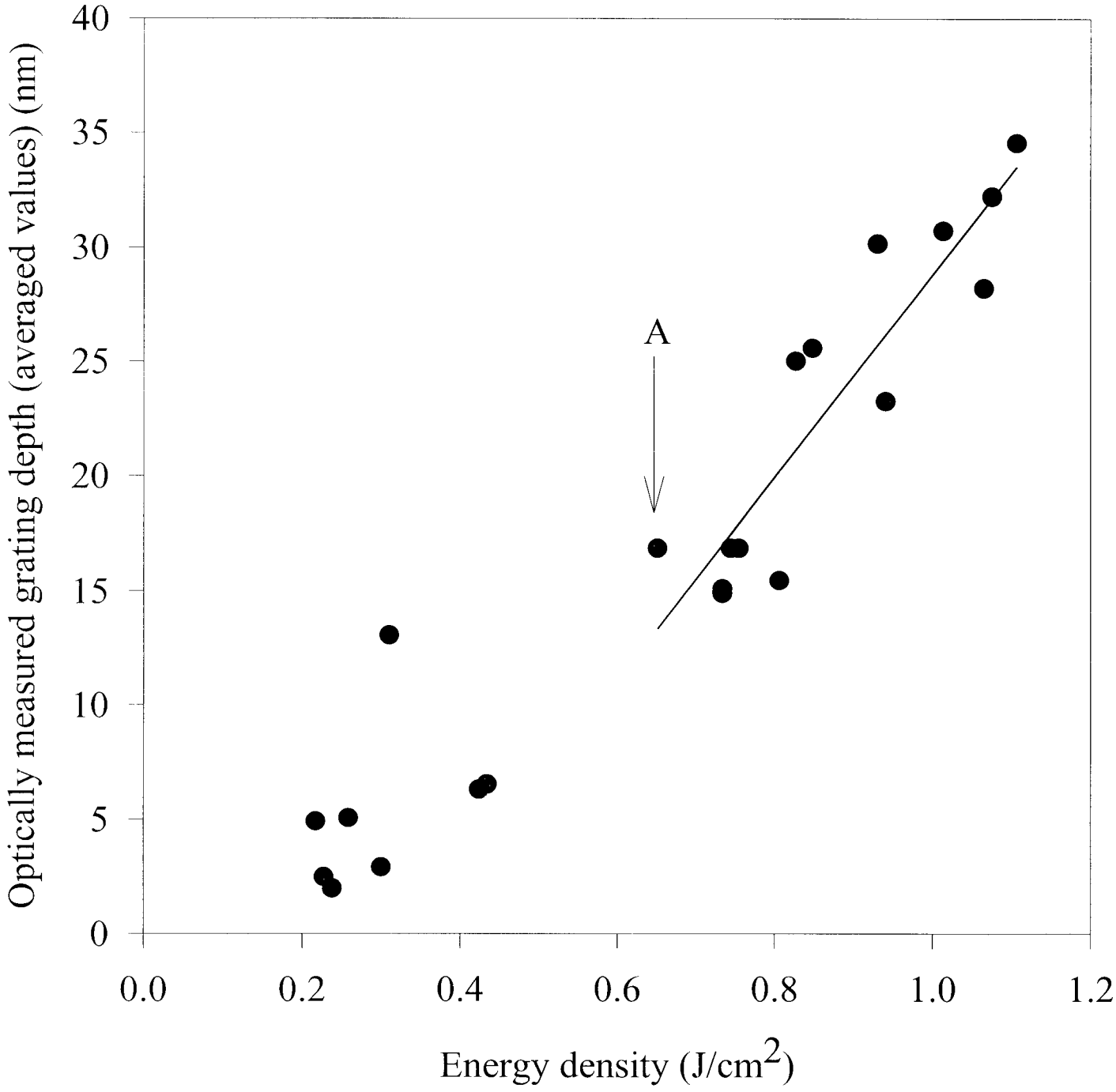
Optically measured grating depth (averaged values) (nm)
40
35
30
25
20
15
10
5
0
A
0.0
0.2
0.4
0.6
0.8
1.0
1.2
Energy density (J/cm2)

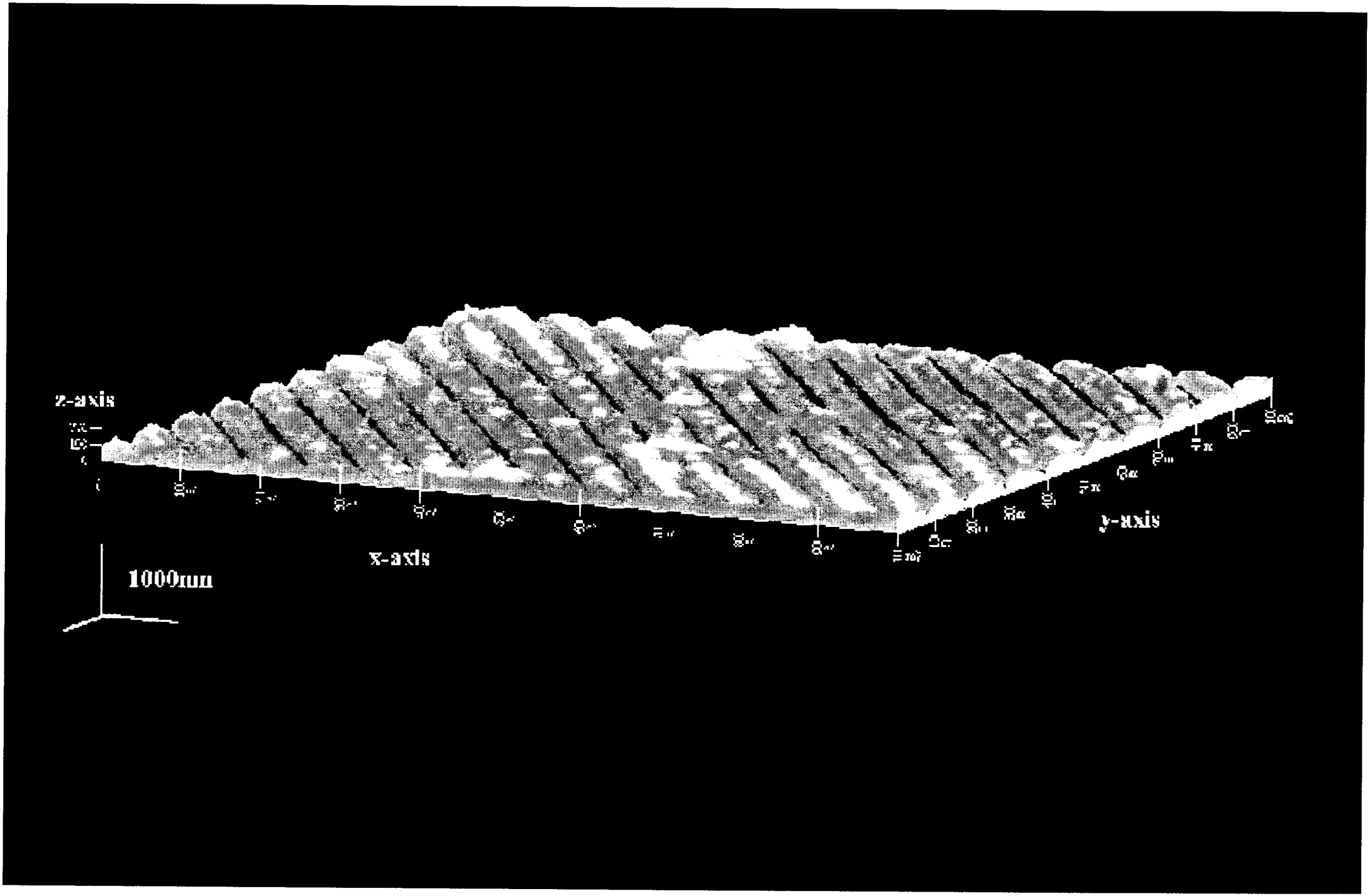

Fig 6

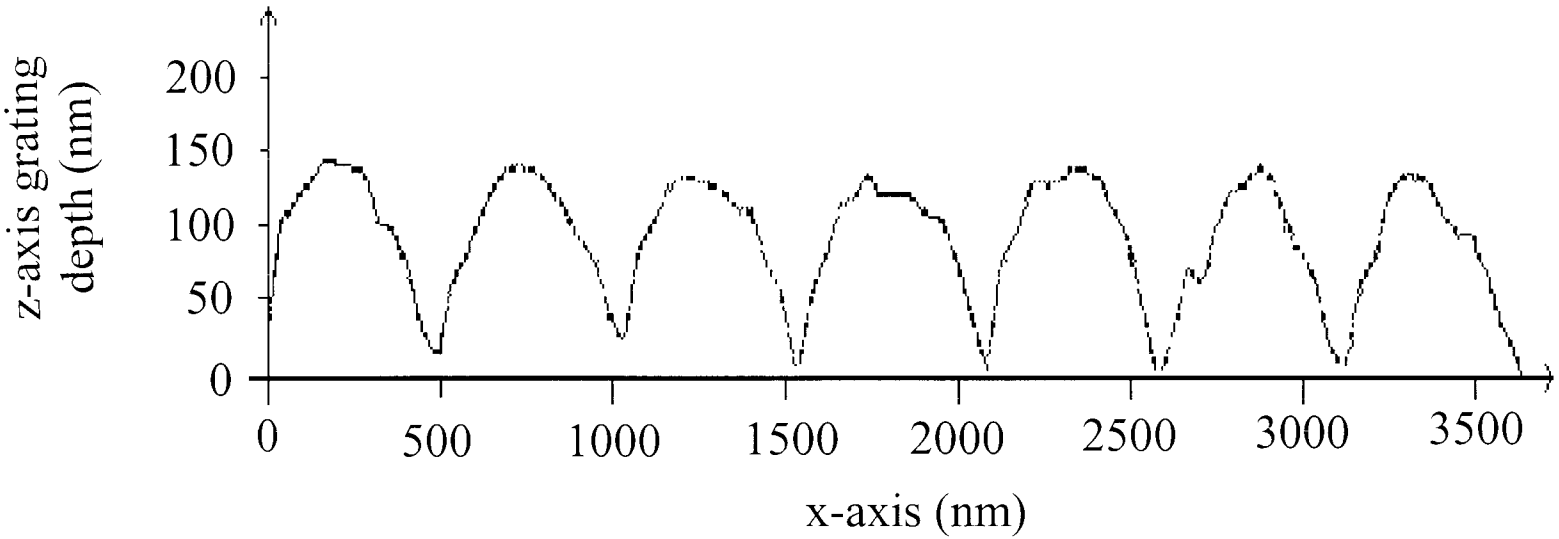
z-axis grating depth (nm)
200
150
100
50
0
0
500
1000
1500
2000
2500
3000
3500
x-axis (nm)

Fig. 7

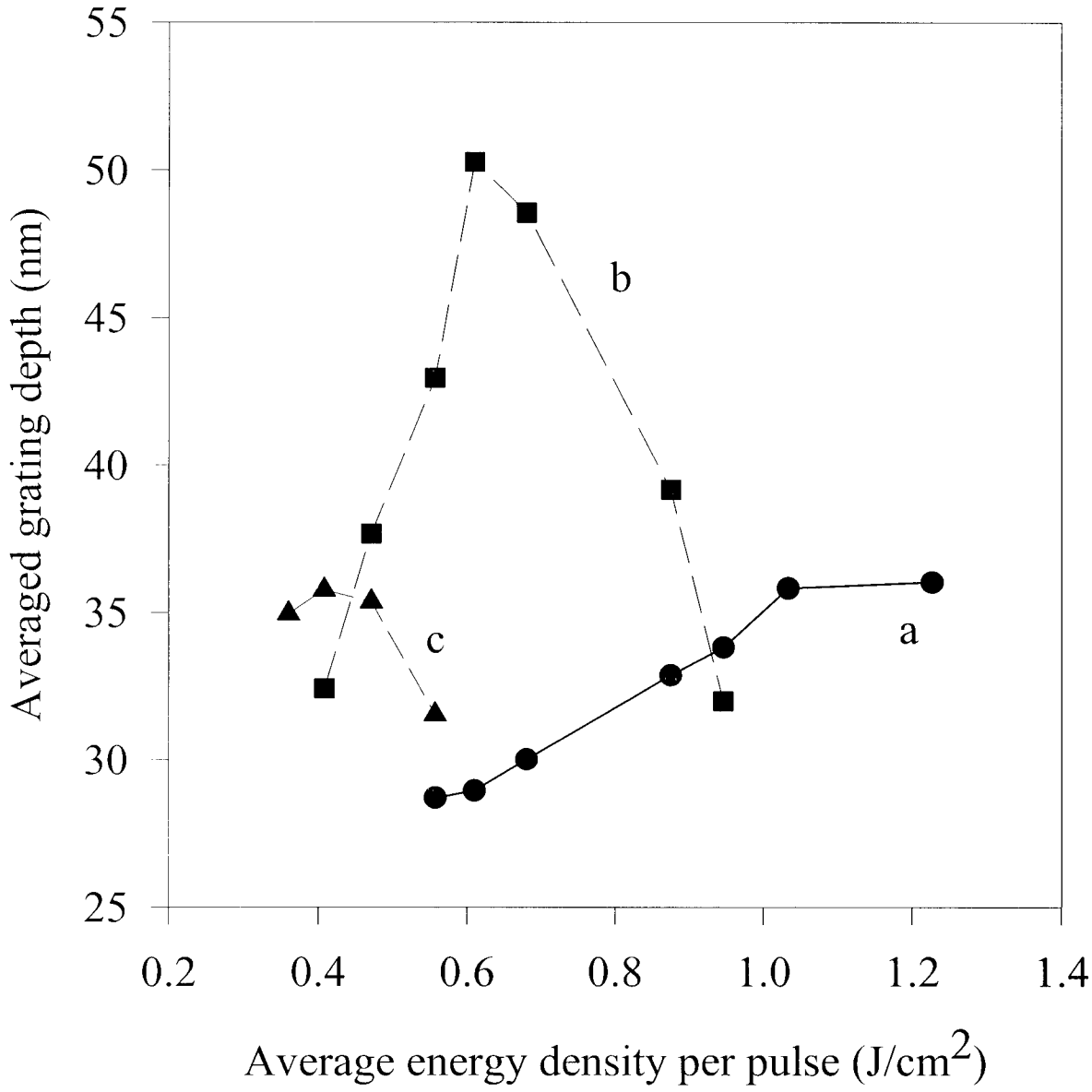
55
50
45
40
35
30
25
Averaged grating depth (nm)
0.2
0.4
0.6
0.8
1.0
1.2
1.4
Average energy density per pulse (J/cm2)
a
b
c

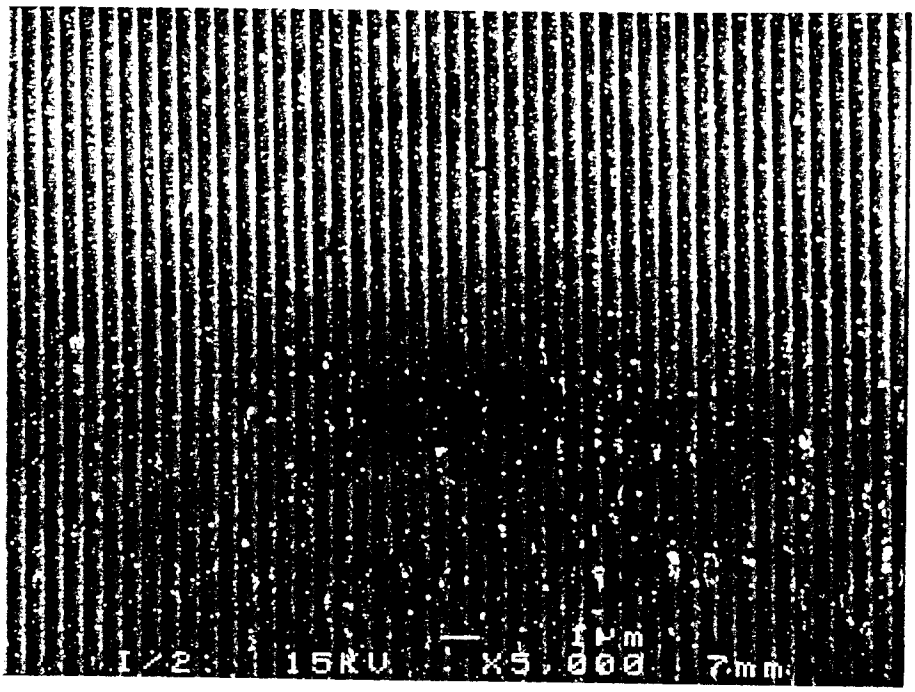
1/2
15KV
X5,000
1μm
7mm

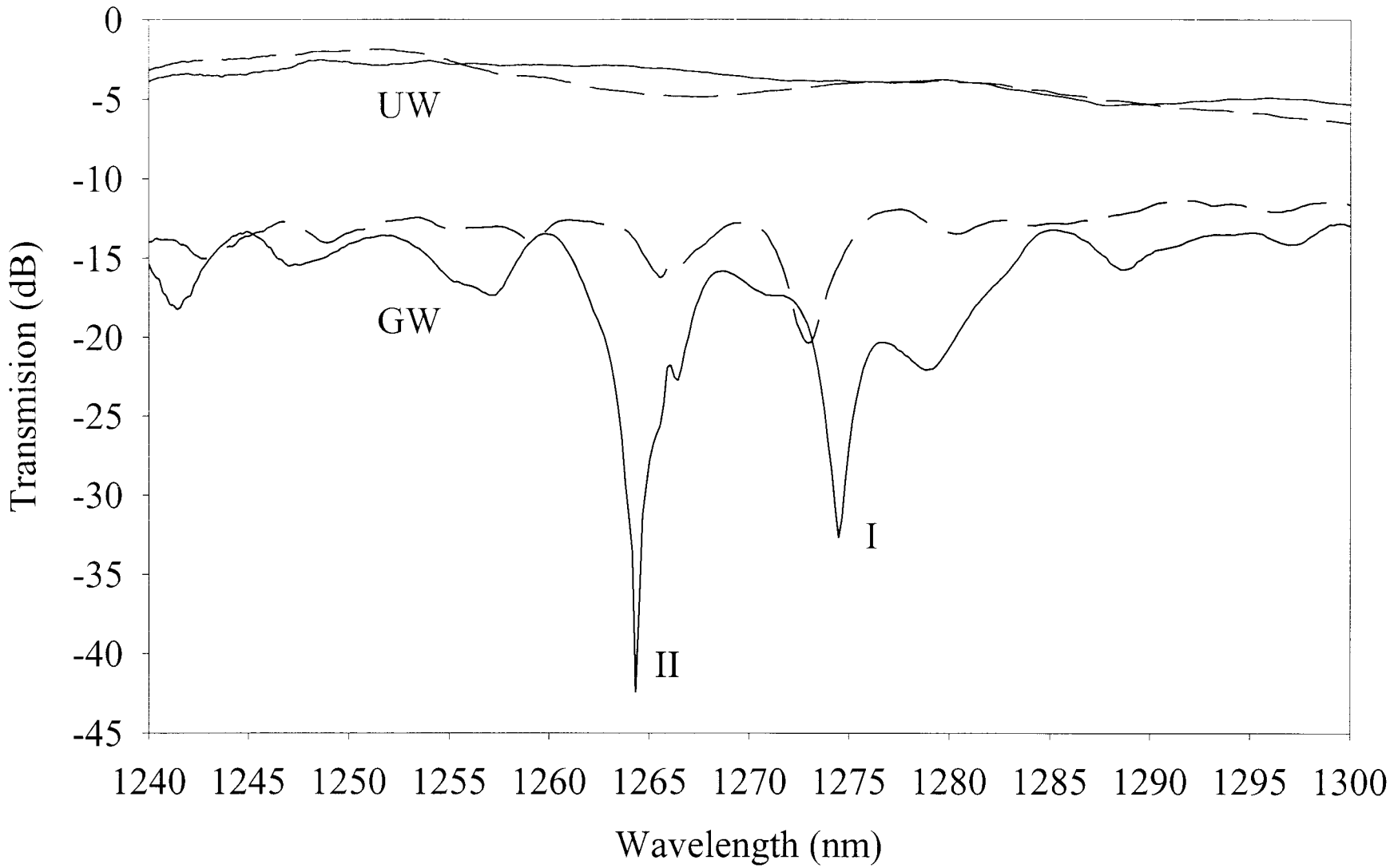
0
-5
-10
-15
-20
-25
-30
-35
-40
-45
Transmision (dB)
UW
GW
I
II
1240
1245
1250
1255
1260
1265
1270
1275
1280
1285
1290
1295
1300
Wavelength (nm)